Comparison of 2-level B6C and 3-level NPC Inverter Topologies for Electric Vehicles

Andreas Bubert
Institute for Power Electronics
and Electrical Drives
RWTH Aachen University
52066 Aachen
Email: post@isea.rwth-aachen.de

Suk-Hyun Lim
Research & Development Division
Hyundai Motor Company
Hwaseong, Korea
Email: sammy.lim@hyundai.com

Rik W. De Doncker
Institute for Power Electronics
and Electrical Drives
RWTH Aachen University
52066 Aachen
Email: post@isea.rwth-aachen.de

***Abstract*—Due to strict emission regulations the electrification of the whole car fleet becomes more and more important resulting in an increased demand for higher powertrain performance and faster dc-charging. One possibility is to increase the dc-link voltage of the electric vehicles. Thus, multi-level inverter topologies are examined considering their suitability for these electric vehicles and compared to standard 2-level inverters. A simulation model to calculate the losses of the inverter was set up, the results were fed into the electric vehicle simulation and used to investigate the efficiency for different driving cycles. In order to validate the simulation results, two inverters were developed using an at most similar design. Furthermore, the fault tolerance was investigated and compared. It could be shown that for new developments in electric vehicles such as high speed electric machines or higher power demand the multi-level topology can be beneficial compared to the standard 2-level topology.**

I. Introduction

Nowadays, most commercial electric vehicles (EV) currently available on the market are designed to be operated with a 400 V dc-link voltage level because both EV manufacturers and customers have focused on small urban vehicles with low power demand rather than other features such as powertrain performance or recharging time. Nevertheless, car manufacturers recently started to electrify their whole fleet including SUV and roadster. Thus, the demand in traction power and lower recharging time increased as well. One way to handle these demands is to increase the dc-link voltage (e.g. 800 V) in order to improve both inverter and powertrain performance and shorten the recharging time of the battery using the existing infrastructure. This change leads to the consideration of other topologies for EV traction inverters, such as Diode-Clamped Neutral-Point-Clamped (NPC) rather than the conventional inverter topology, the so-called 2-Level B6C (controlled six-bridges), shown in Fig. 1a. Although the B6C topology has been dominantly applied into EV traction inverters so far, the need for higher dc-link voltage, which requires higher voltage blocking capability for each switching device, makes other topologies with additional switching levels more attractive. In this paper these two topologies are compared considering their general availability for electric vehicles, efficiency during standard drive cycles and fault-tolerant operation. According to prior studies regarding the implementation of the NPC

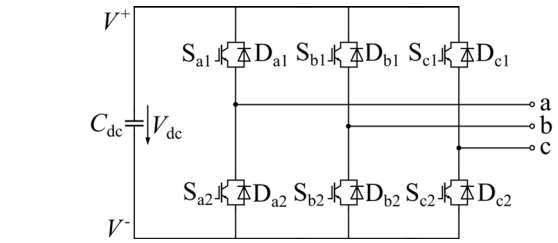

(a) B6C topology

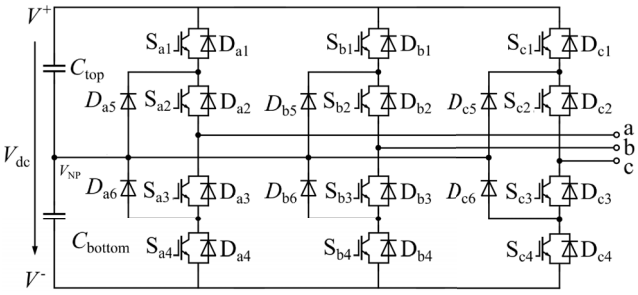

(b) NPC topology

Fig. 1. Examined inverter topologies.

topology into electric vehicle application, it was limited mainly because of the increasing cost compared to the conventional B6C topology for 400 V dc-link voltage, in spite of other benefits. In future EVs with 800 V dc-link voltage switches with 1200 V blocking capability are needed for the B6C, which increases the costs and reduces the efficiency significantly while standard 650 V switches still can be used for NPC. Furthermore, it can be shown that the NPC is advantageous considering efficiency for higher switching frequencies, has lower total harmonic distortion (THD) as well as it has an increased fault-tolerant operation.

II. Fundamentals of B6C and NPC Inverter

Among many well-known inverter topologies, the Diode-Clamped Neutral-Point-Clamped (NPC) topology, shown in Fig. 1b, is selected, because it has been already implemented in many high-voltage applications on the basis of its higher operating voltage, simplicity and reliability while the complexity does not increase significantly in comparison with

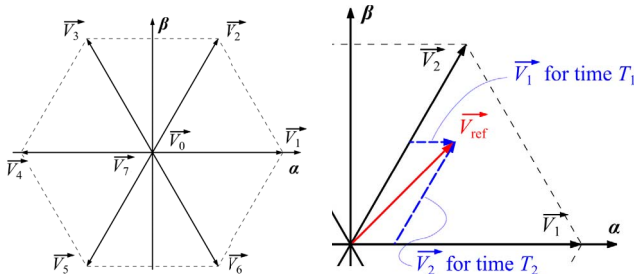

(a) Space vector diagram on $\alpha\beta$-system (b) Synthesis of an example reference voltage vector

Fig. 2. 2-level B6C frequency inverter.

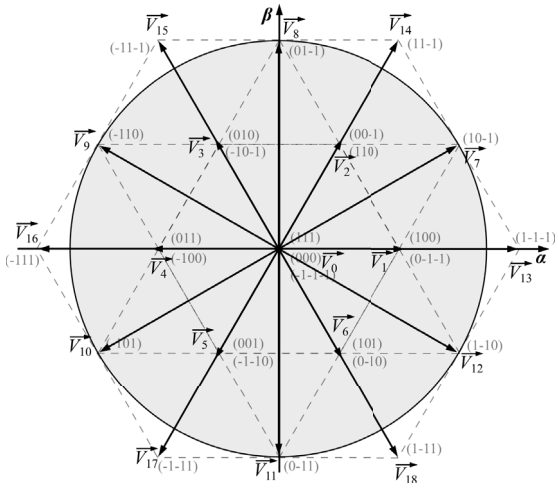

Fig. 3. Space vector diagram of 3-level the NPC converter on $\alpha\beta$-system

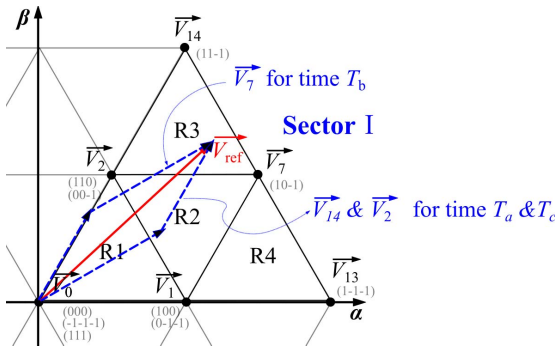

Fig. 4. Synthesis of an example reference voltage vector by the nearest three vectors in the NPC converter

B6C. The NPC, first suggested by A.Nabae, *et al.* in 1981 [1], is a type of multi-level converter which has more than two voltage levels. There are many variations depending on additional components and their connection principle.

The NPC comprises 12 switches (four for each leg) with anti-parallel diodes. There are external switches (S_{x1} and S_{x4}) and internal switches (S_{x2} and S_{x3}). Additionally, the neutral-point (NP) of the dc-link capacitor is connected to a set of clamping diodes (D_{x5} and D_{x6}). The rule of thumb in operation of the NPC inverter is that odd-numbered switches and even-numbered ones are grouped as complementary. For instance, when S_{x1} is ON, S_{x3} must be OFF, and in an opposite way as well to avoid a short circuit.

Depending on the switching states, three different voltages to neutral V_{out} can be generated; V^+, V_{NP}, and V^-. For the sake of simplicity, the first switching state, where S_{x1} and S_{x2} are turned on, is referred to as switching state "1". Similarly, the second and third switching states are referred to as switching state "0" and "-1" respectively. It is clear that switches with a lower (i.e. half) voltage blocking capability can be selected for the same dc-link voltage compared to the B6C inverter.

Pulse-width modulation (PWM) has been widely used in most EV power electronics. Furthermore, space vector modulation (SVM) is used to operate many types of three-phase inverters. SVM is based on the two axis theory to transform the three axis a, b, c into two axis α, β [2]. The idea is that every output voltage can be synthesized by a combination of different space vectors. For the B6C there are in total 7 space vectors (see Fig. 2a) and 8 different switching states (two possible 0 V vectors). By using these space vectors the reference voltage vector $\overrightarrow{V}_{ref}$ can be expressed. For example, if $\overrightarrow{V}_{ref}$ is given (Fig. 2b), the nearest three vectors are selected on the basis of the region where the reference voltage vector is located. Based on the magnitude and the angle of the reference voltage vector, the active times for each vector are calculated as:

$$\overrightarrow{V}_{ref} \cdot T_s = T_1 \cdot \overrightarrow{V}_1 + T_2 \cdot \overrightarrow{V}_2 \qquad (1)$$

For the NPC the possible output phase voltage vectors increase from two to three, the space vector diagram becomes slightly more complex with an additional hexagon layer as shown in Fig. 3. The additional switching state per leg increases the number of available switching states to 27 (three switching states for three-phase legs) while it is eight (two switching states for three-phase legs) in SVM of the B6C converter. It should be emphasized that the number of space vectors is 19 in SVM of the NPC converter with eight redundant vectors. Also it is noticed that all of the 19 vectors can be categorized into four different types, based on their magnitude, i.e. zero, small, medium and large vector, while in the B6C converter they can be separated only in two, i.e. zero vector and non-zero vector. Similar to the 2-level SVM in the B6C converter, the synthesis of a target (reference) space vector $\overrightarrow{V}_{ref}$ by neighboring space vectors is carried out with the 3-level SVM in the NPC converter. Although, the fundamental principle is identical to the 2-level SVM, more space vectors and corresponding switching state options makes the process of space vector synthesis more complex. Furthermore, one of the selected space vectors (the nearest three vectors) for synthesis is not necessarily a zero vector anymore in the 3-level SVM. Additionally, there is a higher degree of freedom and the possibility to use optimized SVM strategies (e.g. [3], [4]) to avoid problems like a jumping neutral point. Using the same method of time-weighting like in the 2-level SVM, if the reference vector $\overrightarrow{V}_{ref}$ is active for a switching period T_s (see

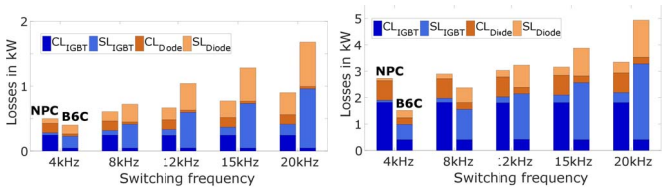

(a) Low speed, low torque (b) Low speed, high torque

(c) High speed, low torque (d) High speed, high torque

Fig. 5. Comparison of the losses in B6C and NPC for different operation points and 5 different switching frequencies.

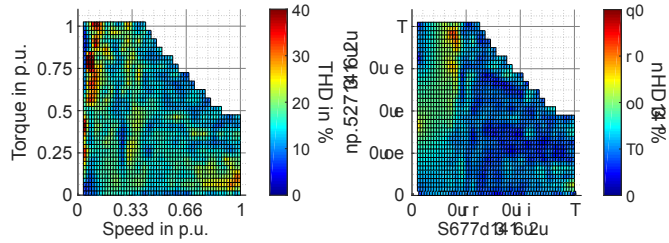

(a) B6C (b) NPC

Fig. 6. Total Harmonic Distortion of the inverter voltage.

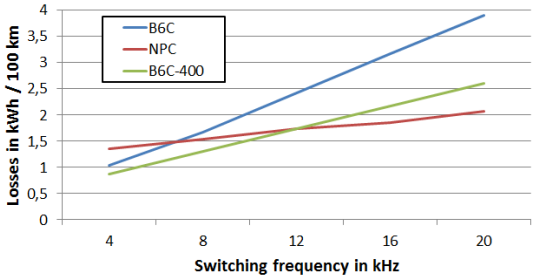

(a) Inverter losses for urban EV

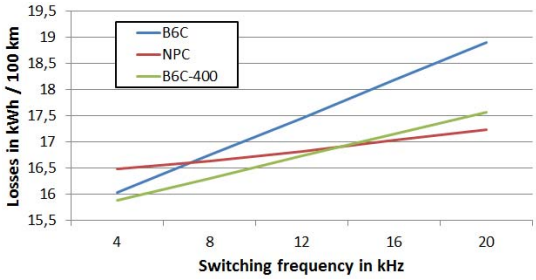

(b) Total losses of the urban EV

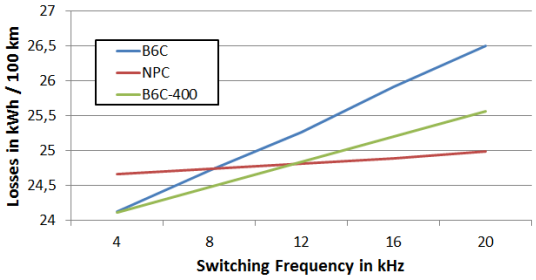

(c) Total losses of the SUV EV

Fig. 7. Simulation results using the EV simulation.

Fig. 4), it can be written as

$$\overrightarrow{V_{\mathrm{ref}}} \cdot T_{\mathrm{s}} = \overrightarrow{V_{14}} \cdot T_{\mathrm{a}} + \overrightarrow{V_7} \cdot T_{\mathrm{b}} + \overrightarrow{V_2} \cdot T_{\mathrm{c}} \tag{2}$$

where T_{a}, T_{b}, and T_{c} are the active time for $\overrightarrow{V_{14}}$, $\overrightarrow{V_7}$, and $\overrightarrow{V_2}$, respectively.

III. Efficiency Comparison of B6C and NPC

Since one of the main focus when developing an EV lies on its range, the efficiency of the powertrain is a key element. In this section B6C and NPC will be compared according to their efficiency.

A. Simulation

The two topologies are simulated using a combined Matlab Simulink and PLECS simulation. The required data and parameters were obtained by measurements (double-pulse experiment) and data sheets from the manufacturer. Fig. 5 shows the simulated inverter losses for four different operation points and five different switching frequencies. The losses are divided in conduction losses (CL) and switching losses (SL) of the diode and switch. As can be seen, for lower switching frequencies the B6C is more efficient than the NPC. Since the EV manufacturers tend to increase the speed of the electric machine in order to reduce its size, the electric frequency increases as well. Thus, low switching frequencies for standard SVM are not feasible anymore.

In a next step, the total harmonic distortion (THD) of B6C and NPC were compared. Fig. 6 shows the result for the whole operation range of the machine. It is clear, that the NPC has a lower harmonic content in almost all operation points. This results in lower losses of the machine and thus increasing the system efficiency of the powertrain.

Since a single operation point does not allow to draw a conclusion about the efficiency of the inverter when it is operated in an EV, a car simulation platform was developed. The simulation consists of all major electrical components of an EV, as well as the chassis and the EV's longitudinal dynamics. A more detailed description of the simulation platform can be found in [5], [6], [7]. The investigated cars are a small EV for urban transportation with a range of 200 km and a SUV with a range of 300 km. The battery is directly coupled to the dc link of the frequency inverter. The gate resistance was chosen according to the data sheet and the double pulse experiment. The electric machine is controlled with a maximum efficiency control strategy [8] and SVM. In Fig. 7 the results of the car simulation for energy consumption of the inverter and the whole EV are shown. It is obvious that already for switching

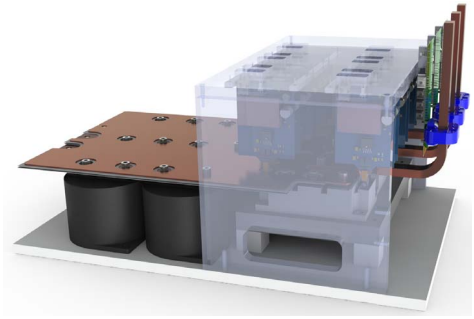

(a) NPC, CAD model

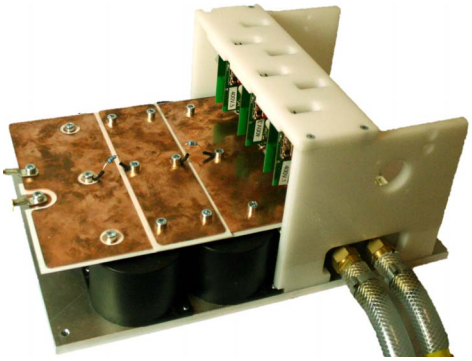

(b) B6C

Fig. 8. Developed frequency inverter with 62 mm modules

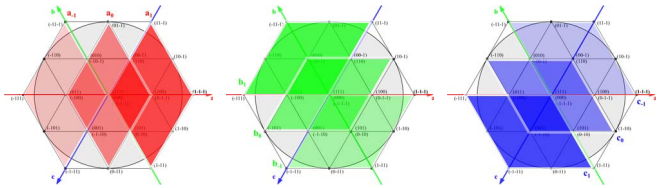

(a) Responsible areas of leg "a" (b) Responsible areas of leg "b" (c) Responsible areas of leg "c"

Fig. 9. 3-level space vector diagram interpreted in three axes (abc) system and responsible areas of each switching state (1,0,-1)

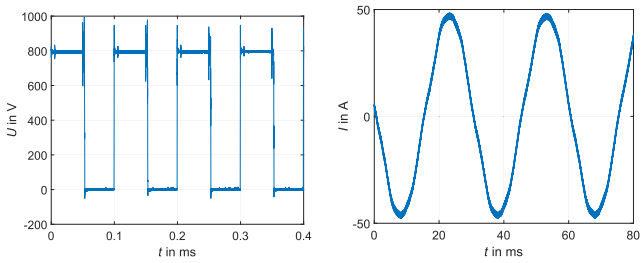

(a) DC-link voltage (b) Phase current

Fig. 10. DC-link voltage and phase current for the regarded operation point for B6C

frequencies above 8 kHz the NPC becomes more efficient. As reference, a comparable B6C with 400 V dc-link voltage was simulated as well. Due to higher currents it is less efficient for higher switching frequencies compared to the 800 V NPC.

B. Measurement

In order to verify the simulation output and get comparable results for the regarded inverter topologies, two inverters (NPC and B6C with 800 V dc-link voltage) were built with a similar set-up (see Fig. 8) by using the same capacitors and module size. The 62 mm modules F300R06KE3 and SKM300MLI066TAT were chosen for the B6C and NPC, respectively. A more detailed description of the inverters can be found in [3]. Fig. 10 shows the voltage (a) and current (b) of the regarded B6C inverter for an measured operation point (approx. 15 % of rated power) with a switching frequency of 10 kHz. Due to delays in the test bench set-up the full operation range couldn't be measured yet. For the regarded operation point the simulated efficiency of the inverter is 91.6 % while the measured efficiency is 91.3 %. When analysing the measuring uncertainties (torque transducer, current and voltage sensors and power analyizer) it can be seen that this deviation of 0.3 % is within this measuring inaccurcy. Thus, for the regarded operation point the simulation shows a sufficient match to the measurements.

IV. Fault-tolerant operation of B6C and NPC

In case of an inverter fault, the EV still should be able to drive to the nearest garage ("limp home"). Fault situations in power electronics switching devices can be categorized as short-circuit (SC) fault, when a switching device remains "ON", and an open-circuit (OC) fault, when a switching device remains "OFF". A detailed categorization can be found e. g. in [9].

Considering the B6C inverter, both SC and OC faults are critical because at least the faulted phase leg must be excluded from operation. Operation with only two phase legs remaining is possible (single-phase excitation), but single-phase operation of an induction machine (IM), especially in EV application, is very limited. In addition to unavoidable pulsating torque production, the single-phase excited IM has no starting capacity in nature. This limitation may be neglected in some applications, but in EV application the operation of a B6C inverter in single-phase excitation mode cannot be considered as a practical method [10]. Therefore, the fault-tolerant operation of the B6C converter without additional components is virtually impossible.

In order to achieve fault-tolerance for both OC and SC fault, the B6C converter requires an additional component for each leg as well as a split capacitors. The additional components are TRIACs (bidirectional triode thyristor) which are connected between the NP of the dc-link capacitors and the mid-point of each phase leg. Once a switch fails, the TRIAC of the faulty leg is activated. However, the increase of part count finally leads to a cost rise by 50 % compared to the standard B6C [10].

In contrast, the fault-tolerant operation of the NPC inverter is available even without additional components (depending on the types of fault). In order to understand the behavior of the NPC, the interpretation of space vector diagram in

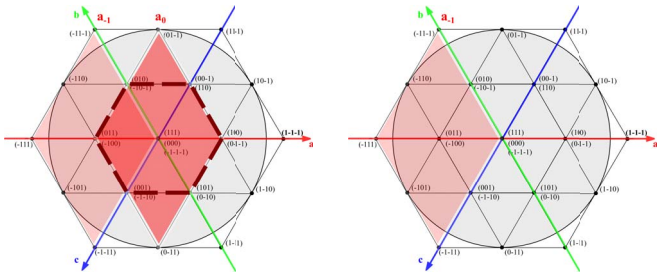

(a) OC fault in the external switch S_{a1}

(b) OC fault in the internal switch S_{a2}

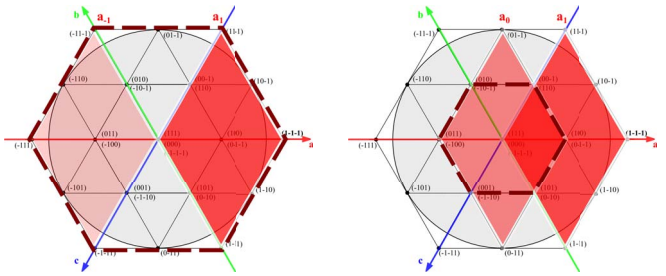

(c) SC fault in the external switch S_{a1}

(d) SC fault in the internal switch S_{a2}

Fig. 11. Elimination of switching status and correspond available vector area by fault type and location

the equivalent three axes (abc) is shown in Fig. 9. Each subfigure presents areas in the space vector diagram where each three possible switching states (1,0,-1) is responsible. This conceptual interpretation can assist the prediction of unavailable switching states under NPC fault conditions. OC faults and SC faults render certain switching states unavailable depending on the faulted switch's index, hence, it is necessary to analyze each type and the location of the fault occurrence. For example, if the external switch S_{a1} (see Fig. 1b) is OC, the switching states involving a turning on of the faulted switch S_{a1}, will not be available anymore. This result gets rid of the diamond-featured area on the right in Fig. 9a. The elimination of the right diamond area reduces the availability of SVM as the area surrounded by the dashed line in Fig. 11a. In consequence, an OC fault in an external switch halves the maximum modulation index. In such a manner, if an OC fault occurs in an internal switch S_{a2}, switching actions involved in turning on the faulted switch S_{a2} will be prohibited in nature. This eliminates the middle and the right diamond area in Fig. 9a. Finally, the available area shrinks as the left diamond area, in which it is not capable to generate a rotating vector starting from the origin. The influence of the OC fault in the external switch can be found in Fig. 11b. Hence, an OC fault in an internal switch is regarded as more fatal fault than OC fault in an external switch.

If the external switch S_{a1} is short-circuited, the switching states involved in turning off the faulted switch S_{a1} will not be available anymore. This leads to the prohibition of the middle diamond area in Fig. 9a, but it does not affect the overall

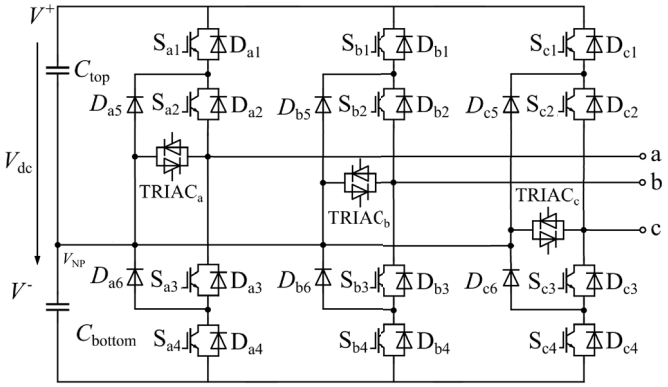

Fig. 12. Configuration of the NPC topology with fault-tolerant capability

boundary of the available area and the maximum modulation index as indicated with the dashed line in Fig. 11c. The only condition to keep the available area is that the blocking voltage of switches in the NPC converter is selected as sufficiently high to withstand a half of dc-link voltage. In this situation, the performance of the NPC inverter would be degraded, because only "1" and "-1" switching states are available which causes increased harmonic contents similar to the B6C inverter. In contrast, when the internal switch S_{a2} is short-circuited, the available area of the space vector diagram and the maximum modulation index accordingly, reduces compared to the SC fault in an external switch. Since the upper capacitor is short-circuited, the switching status of "-1" for the phase leg is not allowed anymore, while the other two status are still available. Even though the number of available switching states remains same as the external switch SC fault case, the available area is biased to the left. Thus, the available area is limited as indicated by the dashed line in Fig. 11d.

As Fig. 11 indicates, except for an OC fault in one of six internal switches of the NPC, all other types of faults are able to be handled properly in order to keep the NPC operating (although it may result in a degraded performance) without modification of the topology itself. In order to continuously run the NPC converter and the EV even with an OC fault in an internal switch, a adaptation to the basic NPC topology is required. A couple of solutions for fault tolerance have already been suggested [11]. The fault-tolerant operation methods can be sorted as '4-leg topology' and '3-leg topology'. The '4-leg topology' suggests an additional leg in order to get some redundancy. This method is simple because it does not require any change in the switching algorithm, but just needs to reset the index of each converter leg. In addition, the performance of the converter will be exactly the same as in pre-fault operation. In spite of its simplicity and high performance, the cost rises accordingly by 30 % compared to the cost of the standard NPC converter [12]. In contrast, the '3-leg topology' only requires a few additional, and cheap, components. Considering the costs, the most feasible '3-leg topologies' can be found in [13], [14]. Instead of an additional inverter leg, three TRIACs are installed as shown in Figure 12.

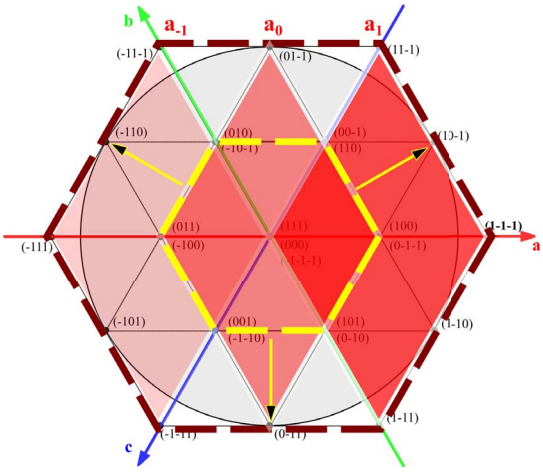

Fig. 13. Expansion of the available area in space vector diagram

Once a SC fault limits availability of a phase leg of the NPC converter, the TRIAC of the faulted leg starts taking the role of an alternative switch. For example, if the internal switch S_{a2} is short-circuited, the TRIAC of leg "a" provides the switching status '0' to the leg "a" for the entire operation so that the available area in the space vector diagram is expanded as shown in Figure 13. In return, the line-to-neutral voltage unbalance problem appears when the NPC converter is modulated by standard SVM [13]. Also, the maximum modulation index decreases by 50 % of normal operation case. However, these handicaps are negligible based on the fact that the main objective of the fault-tolerant operation of the NPC inverter is to guarantee the ability to "limp home" for a short period of time and the output performance is not important, whereas, the additional cost concerns the most. With the fault-tolerant method by TRIACs and fuses, the NPC converter can overcome both OC and SC fault in a single switch with only 10 % cost increase according to [12]. In contrast, the B6C converter with same fault-tolerant ability requires 50 % increase of cost [10].

V. Conclusion

In this work, a comparison between B6C and NPC inverter topologies has been carried out in terms of inverter efficiency, THD, fault tolerance and system efficiency regarding EV applications. B6C and NPC inverter topologies were briefly introduced as well as the space vector modulation of the regarded inverter. It was shown that NPC has advantages considering THD over the whole operation area. Increased electrical frequencies in modern electrical machines makes higher inverter switching frequencies unavoidable. For switching frequencies above 8 kHz the NPC shows a clear superiority to the standard B6C. Since switches used in NPC inverters only need to block half the dc-link voltage, standard 600 V or 650 V modules can be used even for 800 V dc-link voltage. Due to scale effects and high market share of these modules the price of the NPC only increases by 25 % [15] compared to a standard B6C. Taking the advantages of the NPC into consideration (lower THD, lower energy consumption during standard driving cycle and limp-home capabilities), for EV with 800 V dc-link voltage, the NPC inverter is a viable alternative to the standard B6C. Drawbacks such as a fluctuating neutral point can be significantly reduced by optimized modulation strategies.

As next step different modulation strategies will be investigated considering efficiency and dc-link capacitor ripple such as radial state space (RSS) modulation. Furthermore, other benefits of the inverter such as lower THD and its impact on electromagnetic interference and bearing currents will be tested using the developed simulation [16] and test bench.

References

[1] A. Nabae, I. Takahashi, and H. Akagi, "A new neutral-point-clamped pwm inverter," *IEEE Transactions on Industry Applications*, vol. IA-17, no. 5, pp. 518–523, Sept 1981.

[2] R. W. D. Doncker, *Advanced electrical drives: analysis, modeling, control*. Springer Netherlands, 2011.

[3] M. Laumen, A. Lamprecht, M. Schubert, and R. W. D. Doncker, "Optimized space vector modulation for dc link balancing in three level neutral point clamped inverters for electric drives," *For review in 2017 IEEE 12th International Conference on Power Electronics and Drive Systems (PEDS)*, December 2017.

[4] D. Holmes and et al., "An improved virtual space vector modulation scheme for three-level active neutral-point-clamped inverter," vol. 32, no. 10, pp. 7419–7434, October.

[5] A. Bubert, J. Escandon, and R. W. D. Doncker, "Automatic dimensioning of a power converter based on predefined parameters," in *2016 IEEE International Conference on Power Electronics, Drives and Energy Systems (PEDES)*, December 2016.

[6] A. Bubert, P. Kauffmann, A. Au, and R. W. D. Doncker, "Application-oriented design of mechatronic drive-trains," in *2014 IEEE International Conference on Mechatronics and Automation (ICMA)*, August 2014.

[7] J. Becker and T. Nemeth, "Dimensioning and optimization of hybrid li-ion batteries for evs," *EVS30 Symposium*, no. Stuttgart, October 2017.

[8] M. Laumen, A. Lamprecht, M. Schubert, and R. W. D. Doncker, "Synchronous machine model considering dynamic losses and thermal behavior," *2015 IEEE International Electric Machines & Drives Conference (IEMDC)*, May 2015.

[9] R. Wu, F. Blaabjerg, H. Wang, M. Liserre, and F. Iannuzzo, "Catastrophic failure and fault-tolerant design of igbt power electronic converters - an overview," in *Industrial Electronics Society, IECON 2013 - 39th Annual Conference of the IEEE*, Nov 2013, pp. 507–513.

[10] B. A. Welchko, T. A. Lipo, T. M. Jahns, and S. E. Schulz, "Fault tolerant three-phase ac motor drive topologies: a comparison of features, cost, and limitations," *IEEE Transactions on Power Electronics*, vol. 19, no. 4, pp. 1108–1116, July 2004.

[11] W. Zhang, D. Xu, P. N. Enjeti, H. Li, J. T. Hawke, and H. S. Krishnamoorthy, "Survey on fault-tolerant techniques for power electronic converters," *IEEE Transactions on Power Electronics*, vol. 29, no. 12, pp. 6319–6331, Dec 2014.

[12] P. Lezana, J. Pou, T. A. Meynard, J. Rodriguez, S. Ceballos, and F. Richardeau, "Survey on fault operation on multilevel inverters," *IEEE Transactions on Industrial Electronics*, vol. 57, no. 7, pp. 2207–2218, July 2010.

[13] G.-T. Park, T.-J. Kim, D.-W. Kang, and D.-S. Hyun, "Control method of npc inverter for continuous operation under one phase fault condition," in *Industry Applications Conference, 2004. 39th IAS Annual Meeting. Conference Record of the 2004 IEEE*, Oct 2004, pp. 2188–2193 vol.4.

[14] J. J. Park, T. J. Kim, and D. S. Hyun, "Study of neutral point potential variation for three-level npc inverter under fault condition," in *Industrial Electronics, 2008. IECON 2008. 34th Annual Conference of IEEE*, Nov 2008, pp. 983–988.

[15] "Technology and market intelligence: Hybrid vehicle power inverters cost analysis," Report to DOE, 2011.

[16] A. Bubert, J. Zhang, and R. W. D. Doncker, "Modeling and measurement of capacitive and inductive bearing current in electrical machines," in *For Review in 2017 Brazilian Power Electronics Conference (COBEP)*.